ORIGINAL ARTICLE

Automatic virtual reconstruction of maxillofacial bone defects assisted by ICP (iterative closest point) algorithm and normal people database

Bimeng Jie[1,2] · Boxuan Han[3] · Baocheng Yao[1,2] · Yi Zhang[1,2] · Hongen Liao[3] · Yang He[1,2]

Abstract

Objectives The aim of this study was to propose and validate an automatic approach based on iterative closest point algorithm for virtual complement and reconstruction for maxillofacial bone defects.

Materials and methods A 3D craniomaxillofacial database of normal Chinese people including 500 skull models was established. Modified iterative closest point (ICP) algorithm was developed to complete bone defects automatically. The performances were evaluated by two approaches: (1) model experiment, virtual bony defects were created on 30 intact normal skull models not included in the database. For each defect model, the algorithm was applied to select the reference skull model from the database. 3-Dimensional and 2-dimensional comparison were conducted to evaluate the error between reference skull model with original intact model. Root mean square error (RMSE) and processing time were calculated. (2) Clinical application, the algorithm was utilized to assist reconstruction of 5 patients with maxillofacial bone defects. The symmetry of post-operative skull model was evaluated by comparing with its mirrored model.

Results The algorithm was tested on an CPU with 1.80 GHz and average processing time was 493.5 s. (1) Model experiment, the average root-mean-square deviation of defect area was less than 2 mm. (2) Clinical application, the RMSE of post-operative skull and its mirrored model was 1.72 mm.

Conclusion It is feasible using iterative closest point algorithm based on normal people database to automatically predict the reference data of missing maxillofacial bone.

Clinical relevance An automated approach based on ICP algorithm and normal people database for maxillofacial bone defect reconstruction has been proposed and validated.

Keywords Computer-assisted surgery · Iterative closest point · Normal people database · Maxillofacial reconstruction

Bimeng Jie and Boxuan Han contributed equally to this work and share first authorship.

✉ Hongen Liao
liao@tsinghua.edu.cn

✉ Yang He
fridaydust1983@163.com

1 Department of Oral and Maxillofacial Surgery, Peking University School and Hospital of Stomatology, 22 Zhongguancun South Road, Beijing 100081, China

2 National Engineering Laboratory for Digital and Material Technology of Stomatology, Beijing Key Laboratory of Digital Stomatology, National Clinical Research Center for Oral Diseases, Beijing, China

3 Department of Biomedical Engineering, School of Medicine, Tsinghua University, Haidian District, Beijing 100084, China

Introduction

Maxillofacial bone defects after oncological resection and trauma can lead to serious deficits in patient's physiological function and esthetic appearance [1, 2]. The purpose of surgical reconstruction for maxillofacial bone defects is to restore the missing part by autogenous free tissue transfer or artificial prosthetics [3], which requires a high standard of surgical precision to re-establish the function and facial esthetics. Since 2009 [4], computer-assisted surgery (CAS) has been popularly applied to maxillofacial reconstruction and proved to provide better outcomes compared with traditional methods [5, 6].

In CAS, the essential part is acquiring reference data of the missing bone. For unilateral defects, bone data of the unaffected side can be "mirrored" according to the midsagittal plane (MSP) and then used as reference data for

reconstruction [7]. However, accuracy of the "mirror" technique remained ambiguous due to manual selection of MSP, adjustments of the mirrored data, and natural asymmetry of the human skull [8–10]. For bilateral defects, Yao [11] applied a three-dimensional (3D) craniomaxillofacial database to provide reference data. Nevertheless, the matching method was based on manual selection of anatomic landmarks, which was labor intensive and in lack of accuracy.

How to use automatic algorithms to predict the missing bone based on normal people database has been a popular topic for both surgeons and computer specialists. Several studies have successfully used automatic algorithms to complete the missing scapular bone [12, 13]. The iterative closest point (ICP) is an algorithm employed to minimize the difference between two clouds of points [14]. It has been applied to an automatic comparison between two similar medical data [15].

This was the first study using ICP to automatically predict the reference data of missing maxillofacial bone assisted by the 3D craniomaxillofacial database of normal Chinese people. The aim of this study was to propose and validate an automatic approach based on ICP for virtual complement and reconstruction for maxillofacial bone defects.

Materials and methods

Establishment of the 3D craniomaxillofacial database of normal Chinese people

Computed tomography (CT) scans (helix with 1.25-mm slice thickness) (GE BrightSpeed 16-slice CT scanner, UK) of 500 normal Chinese adults were acquired in the Digital Imaging and Communications in Medicine (DICOM) format. The scan range was from the supraorbital ridge to the chin. Normal adults were defined as follows: (1) Chinese individuals older than 16 years; (2) an intercuspal position with a molar neutral relationship and a normal covering; (3) no surgical history, no bone tumor involvement, and no bone fractures or defects; (4) bilateral symmetry, without any visible deformities; (5) no systemic disease violating bone metabolism and development. The patient demographics of the database are shown in Table 1. All patients received CT scan for diagnostic purposes of conditions unrelated to the study, such as salivary gland disease.

CT scans were then imported into ProPlan CMF software (Materialise NV, Leuven, Belgium). 3D reconstruction of the skull model (window width, 500 Hounsfield unit (HU); window level, 100 HU; threshold, 226–3071 (HU)) was performed. Subsequently, the patient's model (in stereolithography (STL) format) was imported into a database developed in association with Tsinghua University**. The aforementioned methods were published in 2019 [11].

Table 1 Patient demographics of the three-dimensional craniomaxillofacial database of normal Chinese people

Characteristic	N
Gender	
Male	241 (48.2%)
Female	259 (51.8%)
Age distribution	
≤ 30	190 (38%)
31–45	144 (28.8%)
46–60	130 (26%)
≥ 61	36 (7.2%)
Ethnicity	
Chinese (Yellow Race)	500 (100%)
Total	500

The ethics committee of Peking University School and Hospital of Stomatology (PKUSSIRB-201837100) approved this study and all participants have signed informed consent paper for using CT scan data for research purpose.

Surface extraction of the 3D craniomaxillofacial database of normal Chinese people

The frontal surface of each skull model was extracted to accelerate the registration process. First, each skull model was imported into Geomagic Control 2014 (Geomagic, NC, USA). After adjusting to natural head position, an osteotomy plan was created perpendicular to the Frankfort plane passing through the P (Porion) point of the bilateral side to cut the anterior part of the skull. Then, the surface data of the anterior part was extracted for later registration (Fig. 1). The definitions of mentioned landmark points are shown in Table 2 and Fig. 2.

Model experiment evaluating the accuracy of the algorithm

The protocol of the model experiment is shown in Fig. 3.

Step 1: creating artificial defects of bilateral zygomatic and naso-orbital-ethmoid region

The virtual bony defects of the zygomatic and naso-orbital-ethmoid (NOE) region were created by unified methods to testify the accuracy of the algorithm. A total of 15 intact male skull models (37.8 ± 14.1 years) and 15 intact female skull models (44.2 ± 14.3 years) (S0) not included in the 3D craniomaxillofacial database were imported into ProPlan CMF software. Two types of defects were incorporated into each intact skull. For zygomatic defects (S1),

Fig. 1 Surface extraction of the 3D craniomaxillofacial database of normal Chinese people. **A** Adjusting the skull model in natural head position. **B** Creating an osteotomy plan perpendicular to the Frankfort plane passing through the P (Porion) point of the bilateral side to cut the anterior part of the skull. **C** Extracting the surface data of the anterior skull
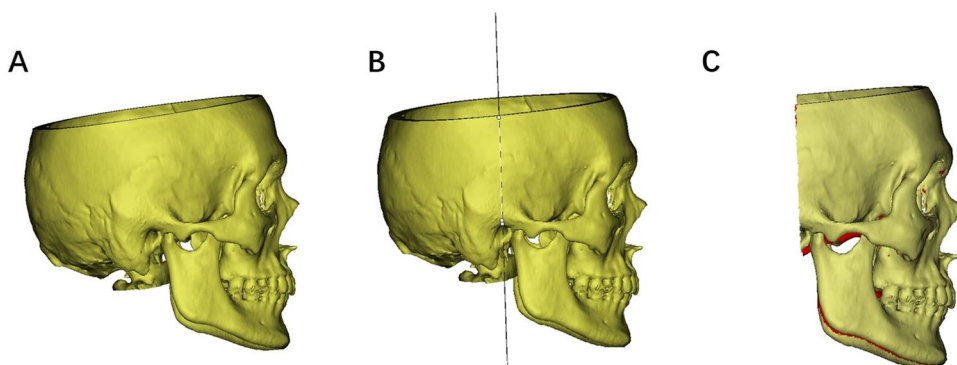
Table 2 Definitions of skull landmark points

Landmark	Description
N (nasion)	The most posterior point on the curvature between the frontal and nasal bones on the midsagittal plane
Mp	The most prominent point of zygoma surface
Fso (foramen supraorbitale)	The center of the superior orbital foramen
Or (orbitale)	The lowest point on the infraorbital margin of right orbit
Zy (zygion)	The most lateral point of zygomatic arch
GL (glabella)	The smooth prominence between the eyebrows
R (rhinion)	The anterior tip at the end of the suture of the nasal bones
Internal canthus ligament (ICL)	The point of internal canthus ligament attachment
Porion (P)	The most lateral point in the roof of the bony external auditory meatus
Sella turcica (S)	The most inferior portion of the hypophyseal fossa

Fig. 2 Scheme illustrations of skull landmark points. **A** Frontal view. **B** Lateral view
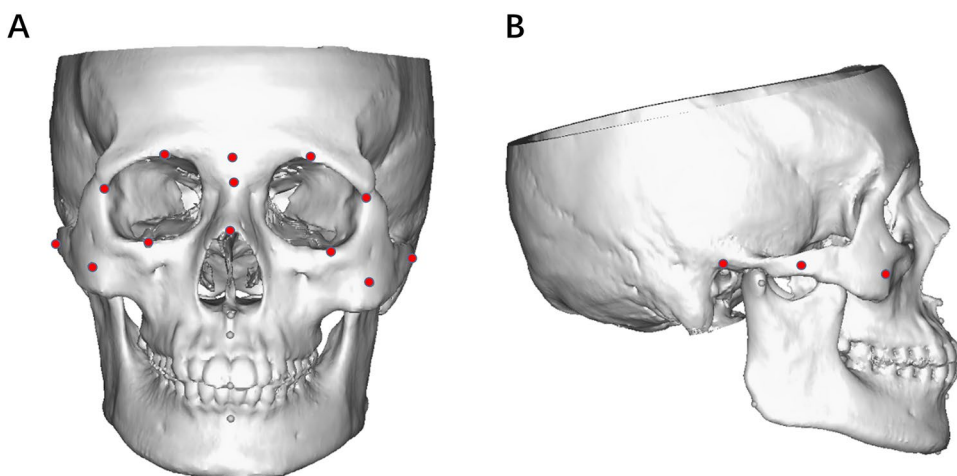
virtual osteotomy planes were created through bilateral zygomaticomaxillary suture, zygomaticofrontal suture, and root of the zygomatic arch. For NOE defects (S2), virtual osteotomy planes were created through the bilateral foramen supraorbitale (Fso) point and orbitale (Or) point (Fig. 4). Then, the anterior surface of each defect skull was extracted in a similar manner.

Step 2: matching reference data similar to the defect data from the database

For each skull defect model, the ICP registration algorithm (Open Source algorithm: https://github.com/PointCloudLibrary/pcl) was applied to select the most similar skull model from the database with the same gender. The deviation of each Euclidean distance between each paired point cloud
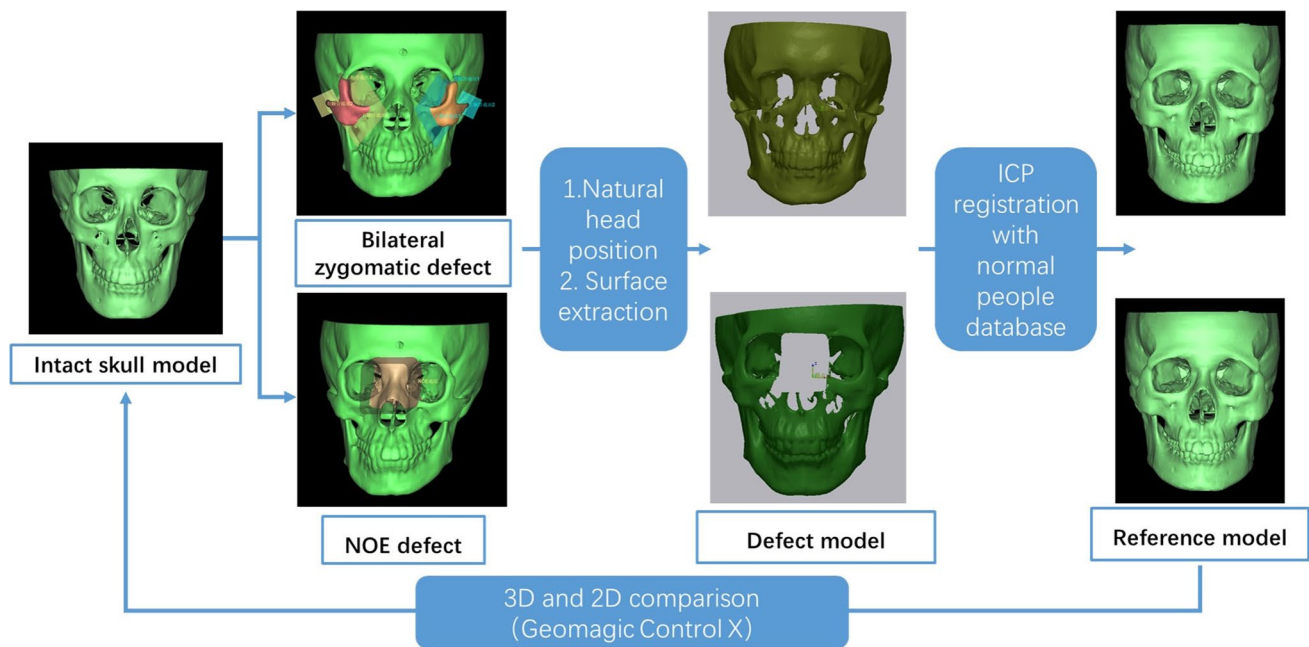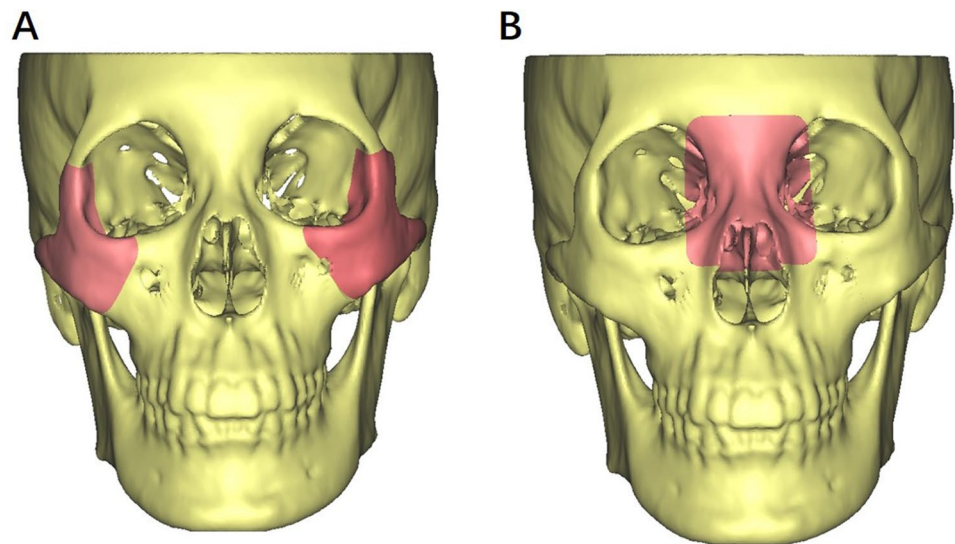
Fig. 3 Protocol of model experiment

Fig. 4 Artificial defects of bilateral zygomatic and naso-orbital-ethmoid (NOE) regions. **A** Virtual osteotomy planes passing through bilateral zygomaticomaxillary suture, zygomaticofrontal suture, and root of the zygomatic arch. **B** Virtual osteotomy planes passing through the bilateral Fso and Or points

present in the defected skull and the normal skull from the database was calculated. The root mean squared error (RMSE) of each model in the database was considered as mean value of the deviation. All models in the database were calculated and ranked in descending order using the ICP algorithm. The model with the lowest RMSE value in the database was exported as the reference data (S1r, S2r). The whole processing time was recorded, and detailed procedures of the ICP algorithm are shown in Supplementary Information S1.

Step 3: comparison of reference data with original intact skull data

S1r, S2r, and S0 were created as STL files and imported into Geomagic Control X 64, (Geomagic, NC, USA). S0 was considered as the ground truth. A 5-mm-enlarged defect area was selected as the superimposed area. The software automatically recognized the corresponding points from the two files and highlighted the superimposed image with different colors according to the distance between the corresponding points. After the comparison, a color-graded error map was
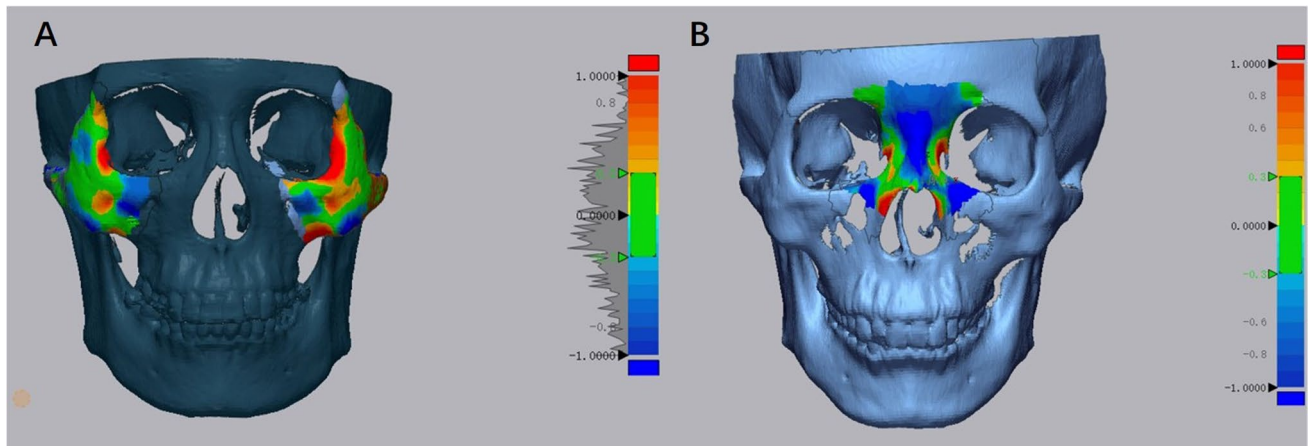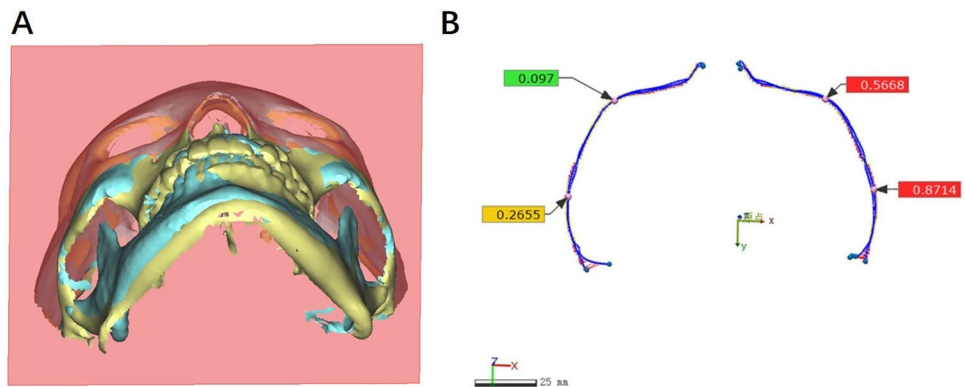
Fig. 5 3D comparison of the defect area. **A** Bilateral zygomatic area of S1r. **B** NOE area of S2r

Fig. 6 2D comparison of the bilateral zygomatic area. **A** Section plane parallel to the Frankfort plane passing through the bilateral Mp point. **B** RMSE of the outer curve and deviation of Mp and Zy points between S1r and S0 were calculated

generated to show the matching deviation between the two files, where each grade of deviation was indicated by a specific color. The distances from the corresponding points in the two files were also automatically measured and analyzed for a comparison report. RMSE was considered as the error of S1r and S2r.

3D comparison The surfaces of the bilateral zygomatic area of S1r and the NOE area of S2r were selected as the 3D comparison areas. RMSE of S1r and S2r was recorded (Fig. 5).

2D curve comparison For the bilateral zygomatic area, the skull model was sectioned by a plane parallel to the Frankfort plane passing through the bilateral Mp point. The outer curve of the section plane was considered as the plane determining the prominence and width of the mid-face. The RMSE of the outer curve and the deviation of Mp and Zy points between S1r and S0 were calculated (Fig. 6).

For the NOE area, the skull model was sectioned by an axial plane parallel to the Frankfort plane passing through the N point and MSP automatically generated using the software. The outer curve of the axial section plane was considered as the width of the NOE area, and the sagittal section plane was considered as the prominence of the NOE area. The RMSE of the outer curve and the deviation of glabella, nasion, rhinion, and bilateral inner canthal ligament (ICL) attachment point between S2r and S0 were calculated (Fig. 7).

All landmark points were defined manually by two experienced maxillofacial surgeons, and the mean deviation was considered as the final result.

Clinical application

Between 2019.10 and 2021.5, the automated algorithm has utilized to assisted reconstruction for 5 patients who received reconstruction of maxillofacial bone defects caused by tumor resection or trauma. The patients (three females, two males) were in the age range of 18 to 57 years (mean, 40.5 years). Table 3 lists the demographic and clinical characteristics of the 5 patients. Written informed consent was obtained from patients before their surgeries.

Fig. 7 2D comparison of the NOE area. **A** Mid-sagittal section plane and deviation of glabella, nasion, and rhinion point. **B** Axial section plane and deviation of bilateral inner canthal ligament (ICL)
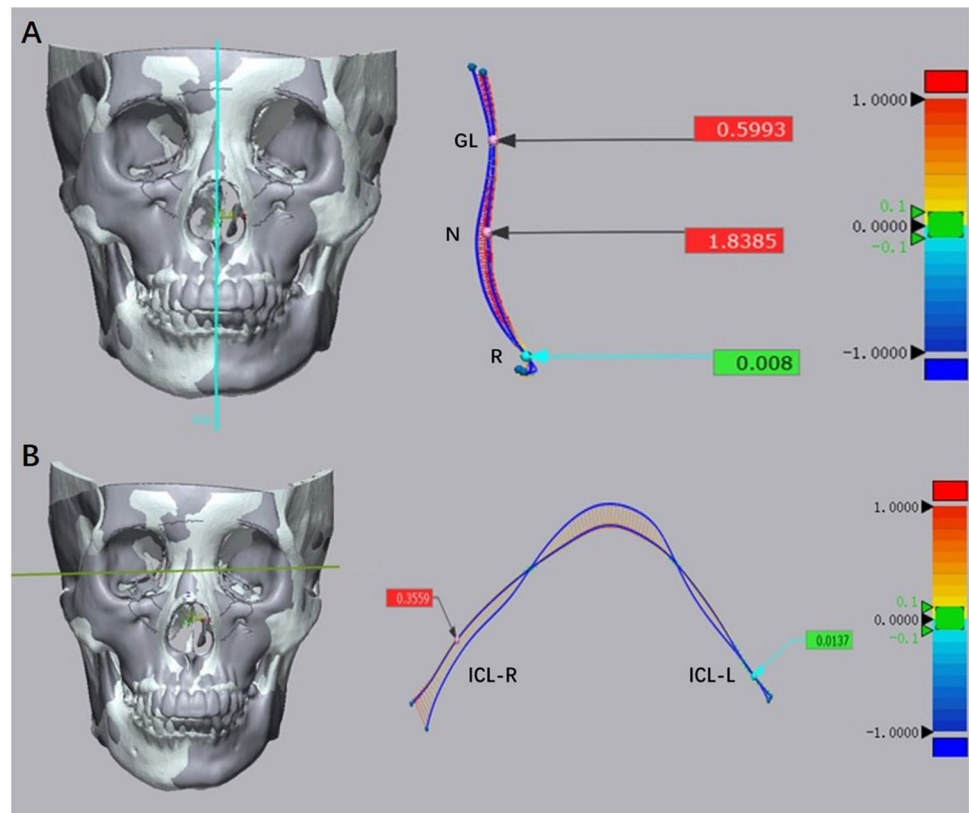
Step 1: virtual surgical planning

Before surgery, preoperative maxillofacial non-contrast enhanced CT scans were acquired (helix with 1.25 mm slice thickness; BrightSpeed 16-slice CT scanner, GE Healthcare, Buckinghamshire, UK). The CT data in DICOM format were imported into ProPlan CMF software. Bone tissue (HU threshold, 226 ~ 3071) were segmented and separately converted to STL file format. The diseased or dislocated bone was removed and the range of defects was then identified.

For each skull defect model, the modified ICP registration algorithm was applied to select the most similar skull model from the database with the same gender (see the "Model experiment evaluating the accuracy of the algorithm" section Step 2). The reference data was then applied to guide the reconstruction plan. According to the reference data, multiple reconstruction methods such as vascularized bone flap were selected to maximally restore bone contour of defect area (Fig. 8D−F).

Step 2: surgical procedure

Fracture reduction, tumor resection, and reconstruction were conducted in one-stage surgery. In order to transfer the preoperative plan, fracture reduction and tumor resection were guided by surgical navigation (Brainlab AG, Feldkirchen, Germany) or 3D printed surgical guides (BTK, Beijing, China) (Fig. 8G−H). The bone flap harvesting was guide by

3D printed surgical guides. The three-dimensional position of bone flap or titanium mesh was confirmed to match the reference data by surgical navigation, pre-bent titanium plate, and 3D printed surgical guides (Fig. 8 I–J).

Step 3: post-operative symmetry evaluation

All patients underwent CT scans at one week after surgery. The post-operative skull was 3D reconstructed and created as STL files using ProPlan CMF. The post-operative model was then imported into Geomagic Control X and mirrored according to mid sagittal plane synthesized automatically by ICP algorithm and principle component analysis(PCA) of the software. 3D color map comparison of post-operative skull and its mirrored model was then conducted. RMSE of the surgical are recorded (Fig. 8K−M).

Results

Model experiment

The algorithm was tested on an Intel(R) Core(TM) i7-8550U CPU with 1.80 GHz. For the bilateral zygomatic area, the mean processing time was 513.9 s for men and 469.7 s for women. For the NOE area, the mean processing time was 525.4 s for men and 464.8 s for women (Table 4).

Table 3 Demographic and clinical characteristics of 5 patients, and the postoperative outcomes

Patient	Sex	Age (years)	Primary diagnosis	Defect location	Reconstruction type	Post-operative symmetry (mm)	Follow-up (months)
1	M	57	Ameloblastoma	Bilateral maxilla	ALT flap + titanium mesh	1.43	24
2	M	33	Delayed zygomatic fracture with defect	Right zygoma and maxilla	DCIA flap	2.17	12
3	M	28	Ossifying fibroma	Anterior mandible	DCIA flap	1.89	6
4	F	18	Ossifying fibroma	Right maxilla	DCIA flap	1.60	1
5	F	68	Adenocarcinoma	Left zygoma and maxilla	DCIA flap	1.52	12

ALT, anterolateral thigh flap; *DCIA*, deep circumflex iliac artery (supplies the iliac crest)

For 3D comparison, the mean RMSE of the bilateral zygomatic area was 1.78 mm for men and 1.80 mm for women, and the mean RMSE of the NOE area was 1.75 mm for men and 1.80 mm for women. For a 2D comparison of the bilateral zygomatic area, the mean RMSE of the outer curve was 1.90 mm for men and 2.04 mm for women. The mean deviation of Mp points was less than 1 mm, while that of Zy points was less than 2 mm. For a 2D comparison of the NOE area, the RMSE of the outer curve representing prominence was 1.59 mm for men and 1.10 mm for women, and the RMSE of the outer curve representing width was 1.75 mm for men and 1.03 mm for women. The mean deviation of glabella, nasion, and rhinion points was less than 2 mm and that of ICL attachment points was less than 1 mm (Table 5).

Clinical application

All surgeries were performed successfully. There were no intraoperative or postoperative complications such as infection, hemorrhage, or facial nerve injury. The average RMSE of surgical area between post-operative skull and its mirrored model was 1.72 mm (Table 3). Figure 8 presents a representative case.

Discussion

Maxillofacial bone defects often result from oncological resection, trauma, and infection, causing severe deficits in patient's function and esthetic appearance. Depending on the complexity of the reconstruction of maxillofacial bone defects, digital surgical techniques have been widely used to achieve customized, minimally invasive, and functional reconstruction [16, 17]. The protocol of virtual surgical planning comprises four main steps: 3D-based image construction and segmentation, acquisition of reference data for reconstruction, identification of defect range and virtual reconstruction, and choice of intraoperative guiding methods [18]. The reference data is considered as the template for later reconstruction, which is the most fundamental and essential part of virtual surgical planning.

Previous studies focused on appropriate but manual ways to obtain reference data. For patients with unilateral defects, the healthy side can be used as a natural reference template for the affected side, which is also known as the "mirror" technique and has been demonstrated to be an effective approach in preoperative planning [19, 20]. However, the accuracy of the "mirror" technique remains ambiguous. The manual selection of the MSP and adjustments of the mirrored data cause an unpredictable systemic error in the reference data, impacting the final result of virtual reconstruction. Bilateral maxillofacial bone defects have no healthy side for applying the "mirror" technique, which has been considered as a contraindication for CAS [21]. In 2019, Yao et al. [11] presented a method for identifying the most coordinated skull model from the 3D craniomaxillofacial database of normal Chinese people as the reference data. However, the manual selection of landmark points was labor intensive, and a systemic error was inevitable.

While pursuing accurate and customized maxillofacial reconstruction, studies have focused on the use of automatic algorithms to predict missing bones as reference data. Image registration refers to obtaining spatial alignment between images of the same or different modalities acquired on the same or different subjects. Registration algorithms were based on corresponding points of 2D-slice images. ICP was a representative algorithm of rigid registration where images only go through translation and rotation changes. ICP was first applied to multimodal image fusion such as MRI and CT in order to compensate disadvantages of single image examination machine [22]. With the development of 3D reconstruction, 3D image registration aiming at aligning two 3D data sets in a common coordinate system was developed. It has been widely used in computer vision, pattern recognition, and CAS. Since first introduced in 1986 [14], the ICP algorithm has been applied successfully in glenoid and scapular reconstruction [12, 13]. Fuessinger et al. [23] proposed a computer-based approach employing a statistical shape model (SSM), an average model formed by points
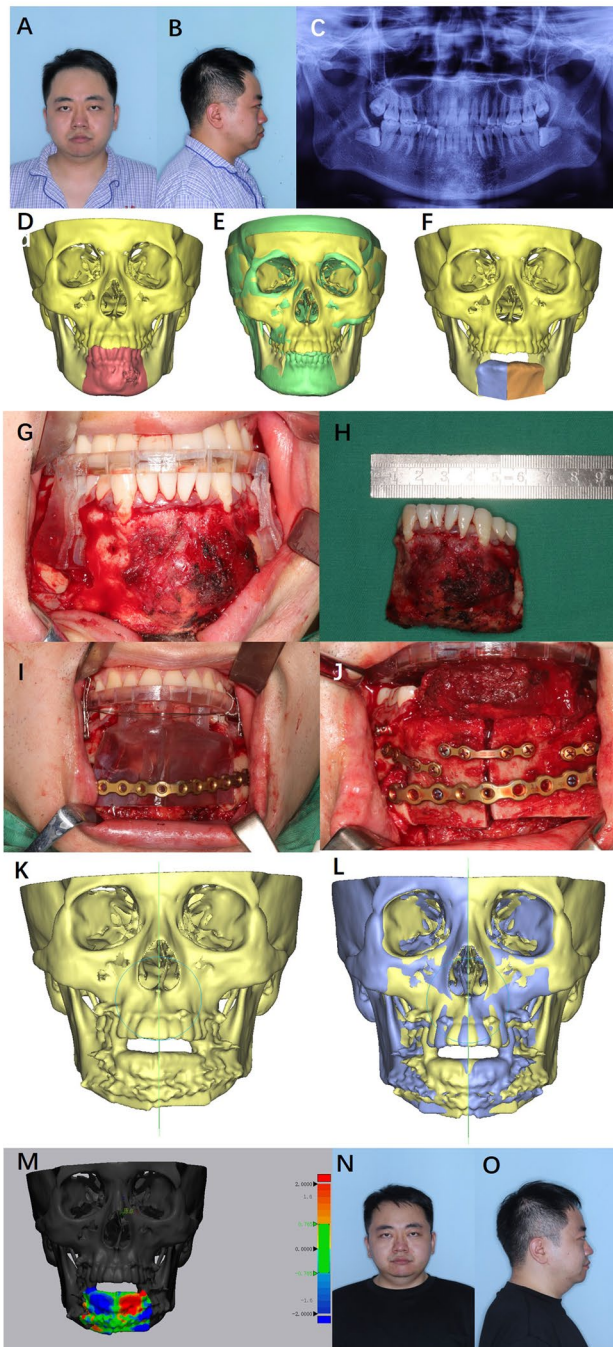
Fig. 8 A representative case of patient No. 3. **A** Pre-operative frontal view. **B** Pre-operative lateral view. **C** Pre-operative panorama showing lesion of anterior mandible. **D** Virtual tumor resection (red). **E** Reference data and automated completion of defect (green). **F** Two-phase DCIA flap reconstruction plan. **G–H** Tumor resection under guidance of surgical template. **I–J** Flap positioning under guidance of pre-bent titanium plate and surgical template. **K** One week post-operative skull reconstructed from CT data. **L** Mirroring of the post-operative skull. **M** 3D comparison of post-operative skull (yellow) and its mirrored model (blue). **N–O** 6 months post-operative photograph showing satisfying appearance

Table 4 Patient demographics and algorithm running time of model experiment (s)

Gender	N	Age (yrs)	Time (s)	
			Zygomatic	NOE
Male	15	37.8 ± 14.1	513.9 ± 90.2	525.4 ± 106.5
Female	15	44.2 ± 14.3	469.7 ± 96.7	464.8 ± 100.1

*NOE, naso-orbital-ethmoid

Table 5 RMSE of model experiment of zygomatic and NOE region (mm)

Characteristic	RMSE(mm)	
	Male	Female
Zygomatic region		
3D comparison		
Bilateral	1.78 ± 0.63	1.80 ± 0.70
Left	1.95 ± 1.04	1.91 ± 0.90
Right	1.61 ± 0.42	1.63 ± 0.58
2D comparison		
Curve	1.90 ± 0.87	2.04 ± 0.92
ZyL	1.83 ± 1.70	1.91 ± 2.07
ZyR	1.82 ± 1.20	1.68 ± 1.90
MpL	0.94 ± 0.63	0.88 ± 0.89
MpR	0.83 ± 0.56	0.92 ± 0.81
NOE region		
3D comparison	1.75 ± 0.82	1.80 ± 0.94
2D comparison		
Curve		
Prominence	1.59 ± 0.78	1.10 ± 0.45
Width	1.75 ± 0.82	1.03 ± 0.60
Glabella	1.27 ± 1.15	0.77 ± 0.73
Nasion	1.22 ± 1.35	0.75 ± 0.62
Rhinion	2.03 ± 1.37	1.42 ± 0.99
ICL-L	0.86 ± 0.59	0.85 ± 0.68
ICL-R	0.82 ± 0.65	0.83 ± 0.63

Abbreviations: *RMSE*, root-mean-square error; *NOE*, naso-orbital-ethmoid; *R*, right; *L*, left; *ICL*, internal canthus ligament

with mean coordinate position of the database, of the cranial vault to acquire reference data. However, SSM without transformation was in lack of characteristics of patient model and the artificial defect only focused on cranial vault with regular shape, which limited the universality of the study. Qiu et al. [24] first combined the ICP algorithm with the Fast Point Feature Histogram to register the defect model point cloud with the patient point cloud. However, this study did not involve the normal people database, and the defect type of the model experiment did not include frequent clinical situations.

The present study was novel in combining the ICP algorithm with the largest scale of the normal people database to recover the missing maxillofacial bone. In order to maximally preserve the characteristics of non-affected area for algorithm calculating, maxilla and mandible were treated as a whole part. Concerns may raise for the unstable position of maxilla and mandible, especially for mandibular defects. During the establishment of normal people database, only normal occlusion with intercuspal position was included. The possible drawback is the relatively low resolution of dentition on the spiral CT data. Accurate dentition data acquired by oral scan will be matched with skull data in future studies.

Due to essential role in facial prominence and width, bilateral zygomatic and NOE areas were selected as artificial defect types in model experiments. The reference skull model data were compared with the original intact skull model, which was considered as the ground truth, to evaluate the accuracy of the algorithm. The 3D comparison was done to evaluate the whole morphology of the defect. The RMSE of the defect area was less than 2 mm, which was equal to the accuracy of navigation-guided surgery [25, 26]. The positions of landmark points determining prominence and width were of more value than the exact surface of the defect because most reconstruction methods involved the use of vascularized bone flaps with a relatively straight contour. Furthermore, 2D comparison of the representative landmark point was then conducted to evaluate the morphology of reference data fully. For the bilateral zygomatic area, Mp and Zy points were considered as landmarks determining prominence and width of the mid-face [27]. For the NOE area, the position of ICL attachment determined the width of the bilateral medial canthus [28]. In the present study, bilateral ICL attachment points were selected as representative points, and the RMSE was satisfying. As for the prominence of the NOE area, glabella, nasion, and rhinion were landmarks determining the lateral appearance of the nasal dorsum. The RMSE of these points showed that the prominence of reference data was similar to the ground truth.

In addition to model experiment, the algorithm was also validated on patients with massive maxillofacial bone defects across the midline. Compared with traditional ways of acquiring reference data, the algorithm automatically extracted unique features of remained healthy bone and common features of the normal people database. Instead of manually selecting mid sagittal plane and adjusting mirrored model, the reference data synthesized by ICP algorithm could be directly utilized to instruct pre-operative reconstruction planning.

Nevertheless, the key drawback of the ICP algorithm was a large number of calculations, leading to more processing time. Considering that the reference skull would serve as a template for the surgical reconstruction of facial contour, the anterior surface of the skull was extracted to accelerate the calculation process. The algorithm was testified on an Intel(R) Core(TM) i7-8550U CPU with 1.80 GHz. Considering the limitations of CPU's calculation ability, the average running time (less than 10 min) was clinically acceptable. However, the accuracy of the ICP algorithm depended heavily on the quality of the original database, leaving less opportunity for later optimization. The reference data acquired by ICP is actually the most similar skull from the database which was not exactly patient-specific. Further studies should be conducted to combine the non-rigid registration algorithm with machine learning to optimize the synthesized reference data.

In conclusion, the ICP algorithm based on the 3D craniomaxillofacial database of normal people was a feasible method to predict the missing maxillofacial bone. The overall processing time was 7–10 min on a basic personal laptop, which was suitable for both surgeons and medical engineers. The accuracy evaluated by the model experiment and clinical application was less than 2 mm, which was acceptable in clinical practice.

Declarations

Ethics approval All procedures performed in studies involving human participants were in accordance with the ethical standards of the institutional and/or national research committee and with the 1964 Helsinki declaration and its later amendments or comparable ethical standards. The ethics committee of Peking University School and Hospital of Stomatology (PKUSSIRB-201837100) approved this study.

Consent to participate Informed consent was obtained from all individual participants included in the study.

Conflict of interest The authors declare no competing interests.

References

1. Brown J, Shaw R (2010) Reconstruction of the maxilla and midface: introducing a new classification. Lancet Oncol 11:1001
2. Brown JS, Barry C, Ho M, Shaw R (2016) A new classification for mandibular defects after oncological resection. Lancet Oncol 17:e23. https://doi.org/10.1016/s1470-2045(15)00310-1

3. Genden EM (2010) Reconstruction of the mandible and the maxilla: the evolution of surgical technique. Arch Facial Plast Surg 12:87. https://doi.org/10.1001/archfacial.2010.18

4. Hirsch DL, Garfein ES, Christensen AM, Weimer KA, Saddeh PB, Levine JP (2009) Use of computer-aided design and computer-aided manufacturing to produce orthognathically ideal surgical outcomes: a paradigm shift in head and neck reconstruction. J Oral Maxillofac Surg 67:2115. https://doi.org/10.1016/j.joms.2009.02.007

5. van Baar GJC, Forouzanfar T, Liberton N, Winters HAH, Leusink FKJ (2018) Accuracy of computer-assisted surgery in mandibular reconstruction: a systematic review. Oral Oncol 84:52. https://doi.org/10.1016/j.oraloncology.2018.07.004

6. Tepper OM, Sorice S, Hershman GN, Saadeh P, Levine JP, Hirsch D (2017) Use of virtual 3-dimensional surgery in post-traumatic craniomaxillofacial reconstruction. J Oral Maxillofac Surg 69:733. https://doi.org/10.1016/j.joms.2010.11.028

7. Zhang Y, He Y, Zhang ZY, An JG (2010) Evaluation of the application of computer-aided shape-adapted fabricated titanium mesh for mirroring-reconstructing orbital walls in cases of late post-traumatic enophthalmos. J Oral Maxillofac Surg 68:2070. https://doi.org/10.1016/j.joms.2009.08.029

8. Pierrefeu A, Terzic A, Volz A, Courvoisier D, Scolozzi P (2015) How accurate is the treatment of midfacial fractures by a specific navigation system integrating "mirroring" computational planning? Beyond mere average difference analysis. J Oral Maxillof Surg 73:315.e1. https://doi.org/10.1016/j.joms.2014.09.022

9. Gui H, Yang H, Zhang S, Shen SGF, Ye M, Schmelzeisen R (2015) Mirroring tool: the simplest computer-aided simulation technology? J Craniofac Surg 26:2115. https://doi.org/10.1097/scs.0000000000000913

10. Gibelli D, Cellina M, Gibelli S, Oliva AG, Termine G, Pucciarelli V, Dolci C, Sforza C (2018) Assessing symmetry of zygomatic bone through three-dimensional segmentation on computed tomography scan and "mirroring" procedure: a contribution for reconstructive maxillofacial surgery. J Craniomaxillofac Surg 46:600. https://doi.org/10.1016/j.jcms.2018.02.012

11. Yao B, He Y, Jie B, Wang J, An J, Guo C, Zhang Y (2019) Reconstruction of bilateral post-traumatic midfacial defects assisted by three-dimensional craniomaxillofacial data in normal Chinese people-a preliminary study. J Oral Maxillofac Surg 77:2302 e1. https://doi.org/10.1016/j.joms.2019.04.030

12. Salhi A, Burdin V, Boutillon A, Brochard S, Mutsvangwa T, Borotikar B (2020) Statistical shape modeling approach to predict missing scapular bone. Ann Biomed Eng 48:367. https://doi.org/10.1007/s10439-019-02354-6

13. Plessers K, VandenBerghe P, Van Dijck C, Wirix-Speetjens R, Debeer P, Jonkers I, Vander Sloten J (2018) Virtual reconstruction of glenoid bone defects using a statistical shape model. J Shoulder Elbow Surg 27:160. https://doi.org/10.1016/j.jse.2017.07.026

14. Horn BKP (1986) Closed-form solution of absolute orientation using uni t quaternions.

15. Xiong Y, Zhao Y, Yang H, Sun Y, Wang Y (2016) Comparison Between interactive closest point and procrustes analysis for determining the median sagittal plane of three-dimensional facial data. J Craniofac Surg 27:441. https://doi.org/10.1097/scs.0000000000002376

16. Hanasono MM, Jacob RF, Bidaut L, Robb GL, Skoracki RJ (2010) Midfacial reconstruction using virtual planning, rapid prototype modeling, and stereotactic navigation. Plast Reconstr Surg 126:2002. https://doi.org/10.1097/PRS.0b013e3181f447e1

17 Foley BD, Thayer WP, Honeybrook A, McKenna S, Press S (2013) Mandibular reconstruction using computer-aided design and computer-aided manufacturing: an analysis of surgical results. J Oral Maxillofac Surg 71:e111. https://doi.org/10.1016/j.joms.2012.08.022

18. Jie B, Yao B, Li R, An J, Zhang Y, He Y (2020) Post-traumatic maxillofacial reconstruction with vascularized flaps and digital techniques: 10-year experience. Int J Oral Maxillofac Surg 49:1408. https://doi.org/10.1016/j.ijom.2020.04.012

19. Zhang WB, Yu Y, Wang Y, Mao C, Liu XJ, Guo CB, Yu GY, Peng X (2016) Improving the accuracy of mandibular reconstruction with vascularized iliac crest flap: role of computer-assisted techniques. J Craniomaxillofac Surg 44:1819. https://doi.org/10.1016/j.jcms.2016.08.014

20 Gellrich NC, Schramm A, Hammer B, Rojas S, Cufi D, Lagreze W, Schmelzeisen R (2002) Computer-assisted secondary reconstruction of unilateral posttraumatic orbital deformity. Plast Reconstr Surg 110:1417. https://doi.org/10.1097/01.PRS.0000029807.35391.E5

21. Lübbers HT, Jacobsen C, Matthews F, Grätz KW, Kruse A, Obwegeser JA (2011) Surgical navigation in craniomaxillofacial surgery: expensive toy or useful tool? A classification of different indications. J Oral Maxillofac Surg 69:300

22. Maintz JBA, Viergever MA (1998) A survey of medical image registration. Med Image Anal 2:1. https://doi.org/10.1016/S1361-8415(01)80026-8

23. Fuessinger MA, Schwarz S, Cornelius CP, Metzger MC, Ellis E 3rd, Probst F, Semper-Hogg W, Gass M, Schlager S (2018) Planning of skull reconstruction based on a statistical shape model combined with geometric morphometrics. Int J Comput Assist Radiol Surg 13:519. https://doi.org/10.1007/s11548-017-1674-6

24 Qiu L, Zhou Z, Guo J, Lv J (2016) An automatic registration algorithm for 3D maxillofacial model. 3D Res 7:20. https://doi.org/10.1007/s13319-016-0083-x

25. Zhang WB, Wang Y, Liu XJ, Mao C, Guo CB, Yu GY, Peng X (2015) Reconstruction of maxillary defects with free fibula flap assisted by computer techniques. J Craniomaxillofac Surg 43:630. https://doi.org/10.1016/j.jcms.2015.03.007

26 Liu XJ, Gui L, Mao C, Peng X, Yu GY (2009) Applying computer techniques in maxillofacial reconstruction using a fibula flap: a messenger and an evaluation method. J Craniofac Surg 20:372. https://doi.org/10.1097/SCS.0b013e31819b9443

27. Gong X, He Y, He Y, An JG, Yang Y, Zhang Y (2014) Quantitation of zygomatic complex symmetry using 3-dimensional computed tomography. J Oral Maxillofac Surg 72:2053 e1. https://doi.org/10.1016/j.joms.2014.06.447

28. Yamamoto H, Morikawa K, Yamashina EU (2001) An anatomical study of the medial canthus using a three-dimensional model. Aesthetic Plast Surg 25(3):189